Applied Geochemistry 119 (2020) 104645

Contents lists available at ScienceDirect

Applied Geochemistry

journal homepage: http://www.elsevier.com/locate/apgeochem

Transfer of FeS-bound arsenic into pyrite during the transformation of amorphous FeS to pyrite

Chao Ma [a,b], Guoping Zhang [a,*], Jingjing Chen [a,b], Qingyun Wang [a,b], Fengjuan Liu [c]

[a] State Key Laboratory of Environmental Geochemistry, Institute of Geochemistry, Chinese Academy of Sciences, Guiyang, 550081, China
[b] University of Chinese Academy of Sciences, Beijing, 100049, China
[c] School of Geography and Tourism, Guizhou Education University, Guiyang, 550018, China

ARTICLE INFO

Editorial handling by Prof. M. Kersten

Keywords:
Arsenic transfer
Iron sulfide
Pyrite
Transformation

ABSTRACT

The transformation of iron sulfide to pyrite is an important process in anoxic environments that strongly influences the mobility of metal(loid)s such as As. It is, therefore, important to understand the fate of As in this process. In this study, batch experiments were conducted at 150 °C and 80 °C and pH 7.5 and 6.0 to examine the transfer of As in the transformation of amorphous FeS to pyrite. The solid phase was characterized using XRD, SEM-EDS, and XPS. The transformation of FeS to pyrite can be promoted in the presence of As(III). During the transformation of FeS loaded with As(III), dissolution of FeS occurs prior to pyrite formation. As(III) is first released in the stage of FeS dissolution, and then is incorporated into the newly formed pyrite. Both high temperature and low pH can promote As uptake by pyrite. XPS analysis indicated sorption as a pathway of As incorporation into pyrite. The contribution from the pathway of lattice substitution is proposed to become significant at high temperature. The results of this study show that As lost or gain in solid phases can occur depending on the As uptake ability by pyrite under different conditions and the initial As loading.

1. Introduction

Under anoxic conditions, sedimentary iron oxides/hydroxides may transform to iron sulfide minerals due to reduction by microorganisms or sulfide produced by sulfate-reducing bacteria (Goldhaber and Kaplan, 1974). Iron sulfides are abundant in freshwater systems, salt marshes, hydrothermal vents, soils, and sediments (Rickard and Morse, 2005). Amorphous FeS is generally thought to be the first formed iron sulfide in aquatic environments (Rickard, 1995). The naturally formed FeS can accommodate significant concentrations of metals and metalloids other than Fe (Morse and Arakaki, 1993). Microorganism-produced FeS is reported to be an excellent sorbent for a wide range of metal ions from solution (Watson et al., 1995). For example, because the mobility of As under anoxic conditions was found to be highly affected by FeS (Wolthers et al., 2005; Gallegos et al., 2007, 2008), many previous studies investigated the sorption or co-precipitation of As by FeS (Wolthers et al., 2005; Xie et al., 2016; Han et al., 2018). In addition to FeS, pyrite is also an important scavenger of metal(loid)s in the environment. Pyrite can incorporate large amounts of As through sorption and lattice substitution. In the mineral structure, As can substitute for sulfur (Savage et al., 2000) or iron (Chouinard et al., 2005) in crystallographic sites. Due to the fact that As can be incorporated into pyrite through multiple pathways, the content of As in pyrite varies to a large extent. The As concentration in pyrite has been reported to be as high as 10.7% (Savage et al., 2000). Huerta-Diaz and Morse (1992) reported As concentrations of up to 0.93 wt% in marine sedimentary pyrite, as inferred from sequential extractions. Kirk et al. (2010) reported an As concentration of 0.84 wt% in newly formed pyrite during microbial reduction of a model aquifer sediment.

Moreover, the high incorporation of As in FeS and pyrite has been used for the remediation of As contamination. Xie et al. (2016) reported the use of FeS coating and biogenic FeS for the in-situ removal of As under reducing conditions. Maguffin and Jin (2018) reported biostimulated sulfate reduction as a strategy for remediating groundwater As contamination. Saunders et al. (2018) reported the bioremediation of As-contaminated groundwater by sequestration of As in biogenic pyrite.

Amorphous FeS is metastable in anoxic sediments (Morse and Arakaki, 1993) and may transform to stable pyrite when a suitable oxidant (e.g., zero-valent sulfur) is present (Benning et al., 2000). Pyrite forms extensively in sediments and the time taken for the average sedimentary framboid to form is about 5 days and the average syngenetic framboid forms within 3 days (Rickard, 2019). Many experimental studies have

* Corresponding author.
E-mail address: zhangguoping@vip.gyig.ac.cn (G. Zhang).

https://doi.org/10.1016/j.apgeochem.2020.104645
Received 6 January 2020; Received in revised form 15 May 2020; Accepted 17 May 2020
Available online 26 May 2020

previously simulated the transformation of FeS to pyrite in the laboratory. It has been demonstrated that pyrite can form via the reaction of FeS with polysulfide (Rickard, 1975; Wilkin and Barnes, 1996) or via the oxidation of FeS by H_2S (Butler and Rickard, 2000). As mentioned above, both amorphous FeS and pyrite are important scavengers of metals and metalloids in the environment, and thus, the transformation of amorphous FeS to pyrite (FeS_2) exerts major control on the geochemical behaviour of As in anoxic sediments. However, the fate of As during the transformation of FeS to pyrite has not been addressed thus far. In a previous study, Wolthers et al. (2007) focused on the impact of the presence of As on the reaction of FeS to form pyrite. In this study, abiotic batch experiments were carried out to simulate the transformation of amorphous FeS to pyrite, so as to elucidate the behaviour of amorphous FeS-bound As in the phase transformation. The initial As(III) concentrations reacted with FeS solids were set to 1, 3.3, 10, 20, 33, and 100 mg/L. A temperature of 150 °C was chosen to simulate the low-temperature hydrothermal formation of pyrite, whereas a temperature of 80 °C was chosen because the abiotic transformation of FeS to pyrite in the laboratory usually becomes difficult below this temperature.

2. Materials and methods

2.1. Materials

Deionized water (DW) (resistivity: 18.2 MΩ-cm) was prepared with a Milli-Q system (Millipore, Bedford, MA, USA). Deoxygenated deionized water (DDW) was prepared by sparging DW with high-purity N_2 (99.99%). Sodium (meta)arsenite ($NaAsO_2$, ≥99.0 purity) was purchased from Sigma Inc. (Mississauga, ON, Canada). Ferrous sulfate heptahydrate ($FeSO_4{\cdot}7H_2O$), sodium sulfide nonahydrate ($Na_2S{\cdot}9H_2O$) and other chemicals were of analytical grade. All solutions were prepared with DDW. Stock solutions of As(III) (500 mg/L), S(–II) (0.2 M), and Fe(II) (0.1 M) were prepared by dissolving sodium arsenite, sodium sulfide nonahydrate, and ferrous sulfate heptahydrate in DDW, respectively.

2.2. Sorption and transformation experiments

The synthesis of FeS and batch sorption experiments were conducted in an anaerobic chamber (Model 855-ACB, PLAS-LANS, CO, USA) at an atmospheric composition of 95% Ar/5% H_2. The residual oxygen inside the chamber was removed by Pd catalysts, resulting in a concentration below 1 ppm.

Amorphous FeS was synthesized by mixing a ferrous solution with a sulfidic solution as described by Jeong et al. (2008). In brief, 1 mL of 0.1 M Fe(II) solution and 1 mL of 0.2 M S(–II) solution were added to a PTFE crucible (ID: 30 mm, height: 55 mm), and amorphous FeS precipitates quickly formed. The freshly precipitated FeS was used for the sorption-transformation experiments and solid phase characterization.

To conduct As(III) sorption by amorphous FeS, a stock solution of As (III) was added. The pH of the solution was adjusted to 7.5 or 6.0 by the addition of 0.1 M HCl and 0.1 M NaOH solution. The initial As(III) concentrations were set to 1, 3.3, 10, 20, 33, and 100 mg/L, and the initial volume of the solution was adjusted to 15 mL through the addition of DDW. The crucible was put on a shaker. The sorption experiment lasted for 24 h. This period was found to be sufficient to reach equilibrium between FeS and As(III) (Gallegos et al., 2007). At the end of the sorption experiment, 2 mL of the mixture were collected and immediately filtered using a cellulose membrane (0.22 μm pore size) for the determination of $As(III)_{aq}$ and $Fe(II)_{aq}$. Then, 0.5 g of elemental sulfur was added to aid in the formation of polysulfide (Licht et al., 1986), and 1 mL of ethanol was added into the mixture to help dissolve the sulfur. To avoid evaporation loss of the solution, the crucible was sealed within a stainless steel tank. Then, the tank was heated in an oven, and the temperature was set to 150 °C or 80 °C to transform FeS to pyrite. The transformation experiment lasted for 24 h. The digestion tank was opened only after cooling down to avoid solution loss by evaporation. Four millilitres of the supernatant were collected, filtered, and then analysed for the concentrations of $Fe(II)_{aq}$ and $As(III)_{aq}$. Seven millilitres of 12 M HCl were added to obtain an HCl concentration of 5 M in the solution. The residual FeS was dissolved, while the crystalline pyrite was resistant to the attack of 5 M HCl (Han et al., 2013). The mixture was separated by centrifugation at 8,000 rpm for 5 min and then the Fe(II) concentration in the supernatant was determined. The Fe(II) in the supernatant comprised both dissolved Fe(II) and FeS-bound Fe(II) after transformation. The solid products separated from the mixture were then immediately washed with DDW and dried using a vacuum freeze drier. The batch sorption and transformation experiments were carried out in triplicate in a parallel mode.

To conduct solid phase characterization of FeS and pyrites, solid samples were separated by filtration in the anaerobic box with a 0.22 m filter and immediately freeze-dried for 24h. Then, solid samples were sealed in a test tube that was filled with N_2 prior to solid phase characterization.

2.3. Analyses

The concentration of $As(III)_{aq}$ was determined by hydride generation-atomic fluorescence spectrometry (HG-AFS) (AFS-2202E, Haiguang Instruments Corp., Beijing, China) following a method of Fu et al. (2016). Regarding the HG-AFS determination, the detection limit for As(III) was 0.03 μg/L. The concentration of $Fe(II)_{aq}$ was measured using a 1,10-phenanthroline spectrophotometric method. The information about procedures adopted to insure quality data are placed in Supporting Information SI.1.1.

2.4. Solid characterization

The mineralogical compositions of the solid products were analysed by X-ray diffraction (XRD) (D-MAX2200, Rigaku Co., Japan). The morphologies and chemical compositions of the solid products were identified by scanning electron microscopy (SEM) (Model JSM-6460LV, JEOL, Japan) in the back-scattered electron mode coupled with energy-dispersive spectroscopy (EDS) (accelerating voltage: 25 kV, EDAX Genesis, USA). The precision and detection limit of chemical composition analysis are 10% and 0.1%, respectively. X-ray photoelectron spectroscopy (XPS, ESCALAB 250Xi, Thermo Fisher Scientific, Inc) was used to determine the solid phase arsenic oxidation state and the relative proportions of different As species. XPS is an important surface-sensitive technique, and the analytical depth is about 0–10 nm. The C1s peak was calibrated according to the standard peak at 284.8 eV. Avantage software (version 5.959) was used for deconvolution and fitting after the Shirley-type background subtraction. The spectra were fitted using an 80% Gaussian and 20% Lorentzian peak model. The semiquantitative composition of the near-surface layers was calculated from the peak areas of the As3d peaks. Narrow-scan spectra were obtained in order to determine oxidation states of As surface species.

3. Results and discussion

XRD pattern for the initial precipitates of FeS in the experiments is shown in Fig. 1. The starting material showed broadened peaks corresponding to those of amorphous FeS. An SEM image of the synthetic FeS is shown in Fig. 2. In general, amorphous FeS was reported to be clusters of nanocrystalline mackinawite (Rickard, 1995; Wolthers et al., 2003) because FeS particles tend to agglomerate rapidly. Typically, the size of FeS particles prepared without a stabilizer ranges from a few nm to 400 nm (Jeong et al., 2008; Wolthers et al., 2005). Some previous studies reported the size of individual FeS particles prepared using the same procedure to be 33 nm (Rickard, 1975), 4.2 nm (Wolthers et al., 2003), and 3.5 nm (Jeong et al., 2008).

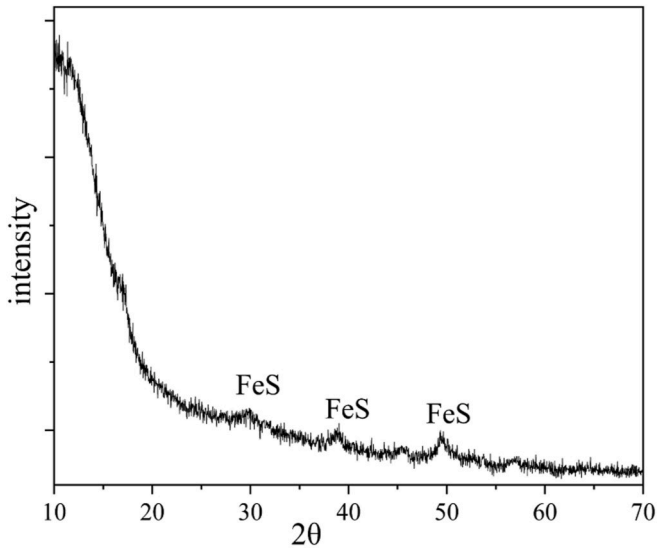

Fig. 1. XRD pattern of the precipitated FeS. FeS labels for disordered mackinawite (JCPDS file 15–0037).

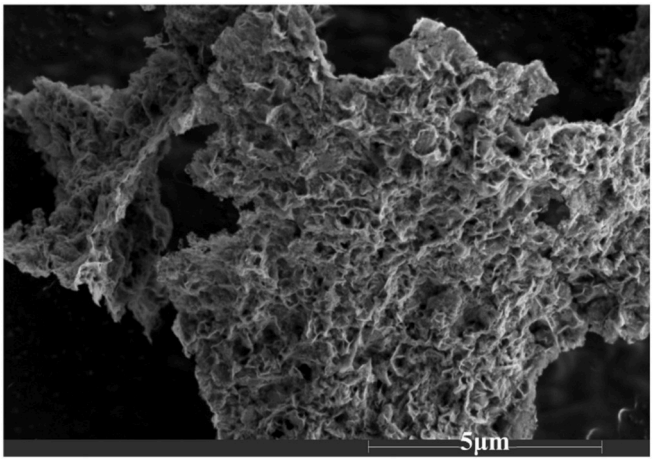

Fig. 2. SEM microphotograph of synthesized amorphous FeS.

3.1. As(III) sorption by FeS

A summary of the experimental conditions and results is shown in Table 1. For the experiments with initial As(III) concentrations of 1, 3.3, 10, 20, 33, and 100 mg/L, the As(III) sorption efficiencies were 87, 84, 83, 88, 93, and 86% at pH 7.5 (averages of experiments 1 and 3) and 88, 84, 83, 93, 95, and 99% at pH 6.0 (averages of experiments 2 and 4), respectively. These results showed that the sorption of As(III) by FeS at pH 6.0 is higher than that at pH 7.5, indicating that a low pH is advantageous in the sorption of As(III) by amorphous FeS. The experiment at pH 6.0 with $As(III)_0$ of 100 mg/L showed the maximum As(III) sorption by FeS of 178 mg As/g FeS. In some previous studies, the maximum As sorption by FeS (unit: mg As/g FeS) was reported to be 128 (Wilkin and Ford, 2002), 1.05 (Bostick and Fendorf, 2003), 9.75 at pH 7.2 (Wolthers et al., 2005), 16 at pH 7 (Han et al., 2011), 28.6 (Xie et al., 2016), and 150 at pH 5 (Renock et al., 2009), respectively. The contrast in the As sorption capacity by FeS can be related to the characteristics of the FeS solids, the initial As concentration, and the pH. In the study of Bostick and Fendorf (2003), troilite (FeS) is the sorbent and the sorption of As is very low.

The solubility of FeS was apparently dependent on the pH (Rickard, 2006), with a greater dissolution at pH 6.0 than that at pH 7.5 (Wolthers et al., 2005). The dissolution of FeS released S(–II) in solution, which reacted with As(III) to form co-precipitation as As_2S_3 on the FeS surface (Farquhar et al., 2002). The co-precipitation as As_2S_3 was related to pH. At a low pH, the solubility of As_2S_3 decreases and the formation of As_2S_3 in a sulfidic system can be promoted (Webster, 1990; Wilkin and Ford, 2002). Consequently, the sorption of As(III) by FeS at pH 6.0 is higher than that at pH 7.5. Similarly, Renock et al. (2009) also reported that As (III) uptake by FeS at pH 5 is substantially greater than at pH 9. Moreover, it has previously been suggested that the surface of FeS has two possible functional groups: an iron (II) hydroxyl functional group $\equiv FeOH^0$ and a sulfide functional group $\equiv SH^0$ (Bebie et al., 1998). With increasing pH, As(III) is present to a greater extent as As bonded to O (As–O) and tends to form $\equiv Fe–OAs(OH)_2$ (Bebie et al., 1998; Farquhar et al., 2002; Gallegos et al., 2007), whereas with decreasing pH, As(III) is bonded to a greater extent with S(–II) in the form of $\equiv S_2–As(OH)$. Therefore, the increase in As(III) sorption at pH 6.0 compared to that at pH 7.5 can also be caused by the formation of ≡SH surface sites, which are the primary functional groups on the FeS surface at lower pH levels.

3.2. The transformation of amorphous FeS to pyrite

3.2.1. Mineral products

Only pure pyrite and untransformed FeS existed in the products. The XRD patterns of the products showed strong peaks that are consistent with pure pyrite (Fig. 3). The SEM analysis showed the morphologies of the pyrites in the experiments (Fig. 4a and b). In the experiments without the addition of initial As(III), cubic pyrites were found, and the particle size was ~500 nm (Fig. 4a). In the experiments in the presence of initial As(III), the pyrite particles were composed of microcrystals (Fig. 4b), and the particle size was mainly <2 μm. This is consistent with the result of some previous studies (Wilkin and Barnes, 1996, 1997; Butler and Rickard, 2000). As shown in SEM-EDS analysis (Fig. 4c and d), Fe and S were the main components in the products. The Fe:S ratio of the HCl-insoluble products was between 1:1.96 and 1:2.06, which is very close to the ideal Fe:S ratio of 1:2 in pyrite (Abraitis et al., 2004). The XRD results and the Fe:S ratio of these products confirmed the formation of pyrite in the experiments.

3.2.2. Transformation

It has previously been suggested that pyrite can form through either the solid state transformation of FeS or direct nucleation from solution (i.e., the solid FeS phase dissolves first). The formation of pyrite inside mackinawite clusters and similarity in size between crystals of the starting and ending minerals were suggested to be consistent with a mechanism of solid state transformation (Stanton and Goldhaber, 1991). When monitoring the transformation of mackinawite to pyrite on polymer supports, Lan and Butler (2014) observed mineral crystals with similar dimensions and co-location of various forms of iron-sulfide minerals. These characteristics were suggested to be consistent with the solid transformation of FeS to pyrite. Lan and Butler (2014) also proposed that non-solid-phase pyrite nucleation occurred based on the observation of both clusters of fibrous particles and small grains of less than 100 nm diameter that had a Fe:S molar ratio similar to that of pyrite. Additionally, as reviewed by Ohfuji and Rickard (2005), the formation of clusters of FeS molecules in solution and nanoparticles of FeS can be involved in the formation of pyrite framboids in sulfidic environments. Rickard (1997) reported that, as a precursor, FeS dissolved first and then reacted to form stable pyrite. Based on a series of pyritization experiments of plant cells, Rickard et al. (2007) confirmed the dissolution of FeS as a key step in the transformation of FeS to pyrite.

The variation in the $Fe(II)_{aq}$ concentration is important for understanding the transformation mechanism. In experiment 3, the conversion rates were less than 74.2% (Table 1), indicating a relatively low consumption of $Fe(II)_{aq}$ by the formation of pyrite. The increase in $Fe(II)_{aq}$ after the transformation indicated that the dissolution of FeS occurred during the transformation. In contrast, $Fe(II)_{aq}$ generally

Table 1
Summary of experimental conditions and results.

Condition	No.	$[As(III)]_0$	After sorption				After transformation				
			$Fe(II)_{aq}$	$As(III)_{aq}$	$[As]_{FeS}$	As sorp.	$Fe(II)_{aq}$	$As(III)_{aq}$	$[As]_{py}$	Conversion	$Fe(II)_{HCl}$
		mg/L	mg/L	mg/L	mg/g	%	mg/L	mg/L	mg/g	%	mg/L
T = 150 °C pH = 7.5	1a	1.0	1.3*	0.1*	1.5	87.1	1.1 *	0.04*	1.2	98.6	5.1*
	1b	3.3	1.7*	0.4*	5.0	86.7	1.3 *	1.2*	2.6	99.5	1.8*
	1c	10	2.2 ± 0.8	1.7*	14.6	83.2	1 *	4.8*	6.6	99.4	2.3*
	1d	20	6.1 ± 2.2	2.9 ± 0.4	30.4	85.7	1.3 *	10.4 ± 1.1	12.3	99.6	1.6*
	1e	33	3.0 ± 1.0	3.0 ± 1.0	52.8	91.0	1.2*	21.8*	14.2	99.5	1.9*
	1f	100	3.1*	14.2 ± 1.0	151	85.8	1.2*	37.3*	79.6	99.6	1.6*
T = 150 °C pH = 6.0	2a	1.0	2.2 ± 0.4	0.1*	1.2	90.0	0.2*	0.02*	1.3	98.6	5.2*
	2b	3.3	3.7*	0.4*	5.1	87.6	0.3*	0.01*	4.2	99.8	0.6*
	2c	10	2.8*	1.5 *	14.9	84.8	0.4 *	0.1*	12.5	99.8	0.6*
	2d	20	2.5*	1.9 *	31.7	90.4	0.4 *	0.04*	25.3	99.9	0.5*
	2e	33	1.52 *	1.8*	54.7	94.7	0.1 *	0.1*	41.7	99.8	0.8*
	2f	100	10.6 ± 3.1	0.8*	178	99.2	0.3*	0.03*	127	99.9	0.4*
T = 80 °C pH = 7.5	3a	1.0	2.0*	0.1*	1.2	87.1	7.8*	0.03*	1.1	44	207*
	3b	3.3	1.4 ± 0.2	0.6*	4.7	80.7	7.5 ± 1.1	2.9 ± 0.3	1.4	39	225*
	3c	10	1.2 *	1.8*	14.4	82.5	9.5 ± 2.7	8.8*	2.4	62.5	138 ± 16
	3d	20	2.6*	1.9*	31.7	90.4	3.2 *	18.4 ± 3.8	3.5	57.7	156 ± 19
	3e	33	1.5*	1.7*	54.9	95.0	5.0 ± 0.8	23.2 ± 2.8	20.3	60.9	144*
	3f	100	2.8*	13.4 ± 3.6	152	86.6	6.0 *	72.7 ± 11	46.5	74.2	95.1*
T = 80 °C pH = 6.0	4a	1.0	1.8*	0.1*	1.5	86.2	1.2 *	0.03*	1.3	82.3	65.5 ± 6.8
	4b	3.3	5.0*	0.6*	4.7	81.1	1.2 *	1.1*	2.3	53	174*
	4c	10	2.1*	2.2*	13.7	78.0	3.6*	2.3*	9.7	91.8	30.2 ± 3.2
	4d	20	4.1 ± 0.8	1.9 *	32	90.8	0.5 *	5.4*	18.3	96.8	11.7 ± 1.9
	4e	33	2.0 *	1.5*	55.3	95.6	1 *	17.3 ± 3.3	19.1	96.3	13.6 ± 1.7
	4f	100	11.6*	1.0*	178	99.0	0.2*	19.6*	101	97.1	10.9 ± 1.6

Note: Initial FeS concentration: 586 mg/L; $[As(III)]_0$: As concentration initially added; $Fe(II)_{aq}$, $As(III)_{aq}$, and $Fe(II)_{HCl}$: measured aqueous Fe(II) and As(III) concentrations and the Fe(II) concentration in a 6 M HCl extract of the transformation products, respectively (expressed as mean ± standard deviation, n = 3. *standard deviation < 10%); $[As]_{Fes}$ and $[As]_{py}$: calculated concentrations of As bound to FeS and pyrite, respectively; conversion (%) is calculated based on Fe that transformed from FeS to pyrite.

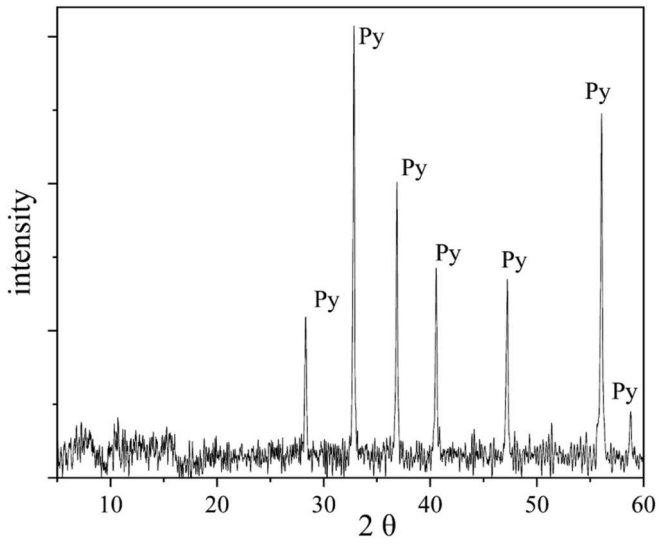

Fig. 3. XRD pattern of the product transformed from FeS. Py labels indicate 2θ-values for diffraction by pyrite (JCPDS file 42–1340).

decreased in experiments 1, 2, and 4 (with the exception of only experiment 4c). This is considered to be caused by the higher conversion of FeS to pyrite that consumed a large amount of $Fe(II)_{aq}$. Similarly, Swanner et al. (2019) reported the dissolution of FeS during the transformation of FeS to pyrite. After the dissolution of FeS, direct nucleation of pyrite nanoparticles from solution can occur (Ohfuji and Rickard, 2005). In the present study, the elemental sulfur reacted with sulfide that originated from partial dissolution of FeS, resulting in the formation of polysulfides. Some previous studies suggested that polysulfides, as intermediates, react with Fe(II) rapidly, resulting in the transformation of FeS to pyrite (Rickard, 1975, 2006). According to the dissolution of FeS and the formation of polysulfides in the experiment, a mechanism of the transformation of FeS to pyrite was proposed as follows (Rickard, 1975, 2006; Wilkin and Barnes, 1996) (S_2^{2-}(aq) represents the polysulfides):

$$FeS + H_2O \rightleftarrows Fe^{2+}(aq) + HS^-(aq) + OH^- \quad (1)$$

$$HS^-(aq) + S^0 + OH^- \rightarrow S_2^{2-}(aq) + H_2O \quad (2)$$

$$Fe^{2+}(aq) + S_2^{2-}(aq) = FeS_2 \quad (3)$$

In this mechanism, dissolution of FeS is involved. The released sulfide is oxidized by S(0) to form polysulfides, and the polysulfides react with $Fe(II)_{aq}$ to form pyrite.

Nucleation and crystal growth are two key processes for the formation of pyrite (Lamer, 1952; Wilkin and Barnes, 1997). It is possible that pyrite initially nucleates as nanoparticles (Qian et al., 2010), and then, the particles grow (Lamer, 1952; Wilkin and Barnes, 1997). In the present work, the particle size of the formed pyrite ranged from ~500 nm to 2 μm (Fig. 4a and b), indicating the growth of pyrite particles after nucleation. The gradual dissolution of FeS supplied the $Fe(II)_{aq}$ required for pyrite growth (Rickard et al., 2007).

The conversion rates based on iron that transformed from FeS to pyrite are shown in Fig. 5. When the pH and initial As(III) concentration remained constant, the conversion rates of the experiments at 150 °C (experiments 1 and 2) were significantly higher than those at 80 °C (experiments 3 and 4). This finding indicates that a high temperature is conducive to the transformation of FeS to pyrite, possibly because the reaction speed can be accelerated at high temperature (Ohfuji and Rickard, 2005; Qian et al., 2010). Further, the solubility increases at high temperature (Benning et al., 2000), resulting in more $Fe(II)_{aq}$ that has been proven to promote the formation of pyrite (Peiffer et al., 2015).

The transformation of FeS to pyrite is also related to pH. When the temperature and $As(III)_0$ remained constant, the conversion rates of the experiments at pH 6.0 were significantly higher than those at pH 7.5 (Fig. 5), indicating that a low pH is conducive to the transformation of

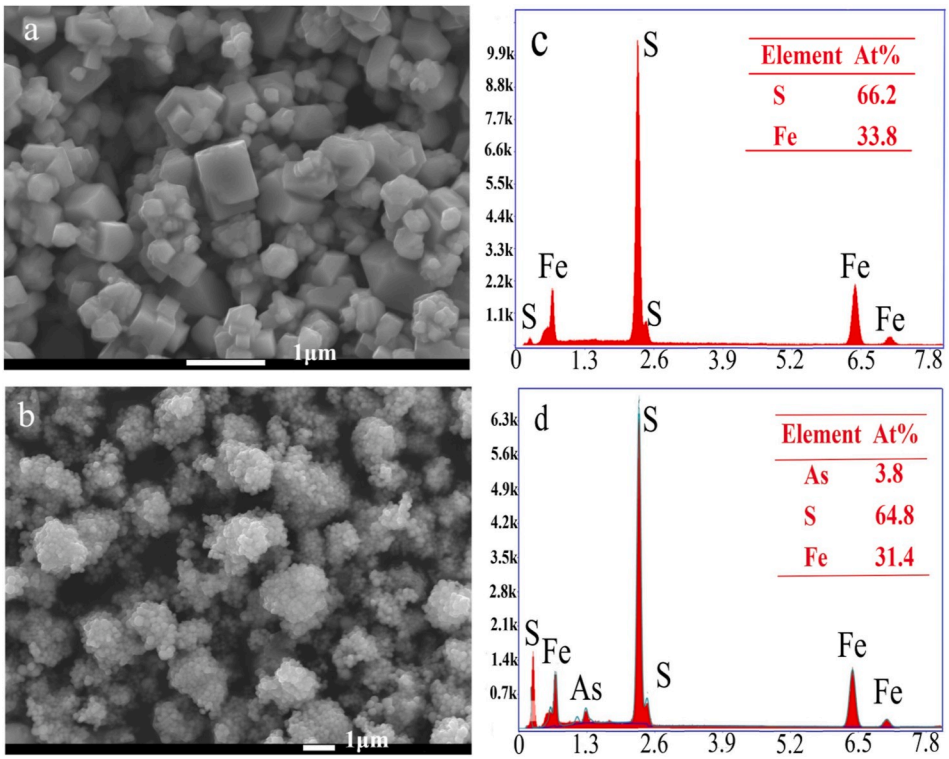

Fig. 4. SEM image and EDS results of pyrite transformed from FeS synthesized in the absence (a and c) and presence (b and d) of As.

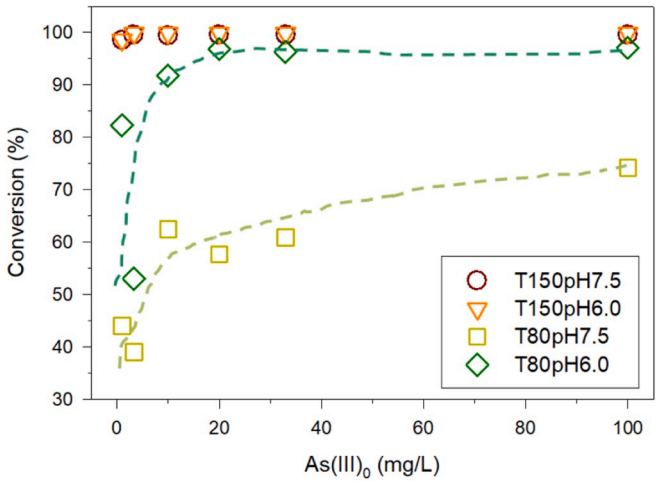

Fig. 5. Impact of the initial As concentration on the conversion rate.

FeS to pyrite. Similarly, higher conversion rates at lower pH have also been reported in previous studies (Wilkin and Barnes, 1996; Rickard, 1975; Schoonen and Barnes, 1991). This is suggested to be related to the role of H^+. First, H^+ can act as an oxidant that is required in pyrite formation (Wilkin and Barnes, 1996; Benning et al., 2000). Second, low pH can promote the dissolution of FeS and result in the generation of more $Fe(II)_{aq}$ (Wolthers et al., 2005; Han et al., 2018), which subsequently promotes the formation of pyrite (Peiffer et al., 2015).

The presence of As(III) also affected the transformation of FeS to pyrite. In experiments 1 and 2 (150 °C), the nearly complete conversions (Fig. 5) made them unsuitable to make a comparison of the difference in the conversion rates. In experiments 3 and 4 (80 °C), the conversion rates varied significantly and an increase in $As(III)_0$ generally corresponded to an increase in the conversion rate. This finding indicates that the presence of As(III) enhanced the transformation. First, As(III) may act as an oxidant that is required for pyrite formation (Schoonen and Barnes, 1991). In this case, As(III) played a similar role to S(0) in the reaction (2). For example, As(III) on the surface of FeS can oxidize S(–II) to disulfide, resulting in the transformation of a fraction (nearly 30%) of FeS to pyrite (Bostick and Fendorf, 2003). This notion is also consistent with the XPS results that indicate the reduction of As(III) to As(II) on the surface of pyrite (see below). Second, the presence of As(III) can induce the dissolution of FeS through the formation of As_2S_3 on the surface of FeS (Farquhar et al., 2002; Wolthers et al., 2005), and the consequent increase in $Fe(II)_{aq}$ has been proven to enhance the kinetic conversion of FeS to pyrite (Peiffer et al., 2015). In contrast to this work, Wolthers et al. (2007) reported that As(III) hindered the transformation of FeS to pyrite because the sorption of As(III) on FeS blocked the active point position on the FeS surface, thereby preventing the ageing of FeS and the subsequent transformation to pyrite. In the present study, the reaction process was a polysulfide pathway due to the addition of S(0), and FeS dissolution occurred during the formation of pyrite. In the study of Wolthers et al. (2007), FeS transformed to pyrite through the oxidation of FeS by H_2S. Thus, the contrast between the result of our study and that of Wolthers et al. (2007) can be attributed to the different mechanisms involved in the FeS transformation to pyrite.

3.3. Speciation of As in the product pyrite

Fig. 6 shows the XPS As-3d spectra of solid products of experiments 1-4f. The doublets of As-$3d_{3/2}$ and $3d_{5/2}$ peaks with a spin-orbital splitting of 0.70 eV were used for fitting As-3d spectra (Nesbitt and Muir, 1998; Kim and Batchelor, 2009). The full-width-at-half-maximum (FWHM) values for all of the model compounds were constrained to be 0.8 eV for low pass energy scans and 2.2 eV for the high pass energy scans. The information about XPS fit results are placed in Supporting Information Table S2.

As shown in Fig. 6, in sample 1f, the relative surface contents of As in the form of As(II)–S and As(III)–O were 6.6% and 93.4%, respectively; in sample 2f, the relative surface contents of As in the forms of As(II)–S, As (III)–O and As(V)–O were 31.2%, 4.3% and 64.5%, respectively; in

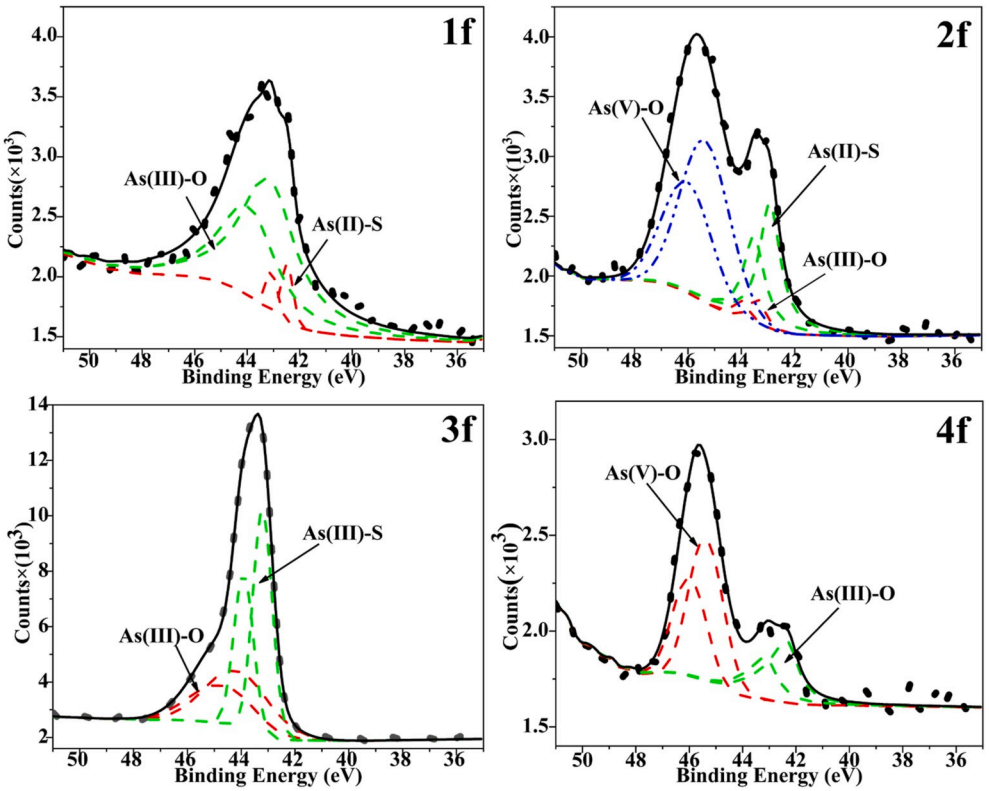

Fig. 6. XPS spectra of As 3d peaks for amorphous FeS reacted with 100 mg/L As(III) for 24 h: (1f) T = 150 °C, pH = 7.5; (2f) T = 150 °C, pH = 6.0; (3f) T = 80 °C, pH = 7.5; and (4f) T = 80 °C, pH = 6.0. As 3d experimental peak fitted with peaks corresponding to As species shown in the figure (dashed lines). Points are the experimental data. The solid line represents the sum of the component peaks.

sample 3f, the relative surface content of As in the form of As(III) was 100%; in sample 4f, the relative surface contents of As in the form of As (III)–O and As(V)–O were 36.0% and 64%, respectively.

As a redox-sensitive element, arsenic will be incorporated into pyrite in different valence states and chemical bonds. The chemical bond of As (III)–O was observed in all samples (1-4f), reflecting the As(III) sorption on the surface of pyrite. Sorption of As can occur when pyrite initially nucleates and then the pyrite particle grows. The chemical bond of As (II)–S existed in samples 1f and 2f (150 °C) while it was not observed in samples 3f and 4f (80 °C), indicating that As(III) reduction to As(II) by S (–II) in the transformation was significant at 150 °C and was minimal at 80 °C. As(III) sorbed on the surface of pyrite can be reduced to As(II) with the oxidation of Fe(II) and S(–I) (Bostick and Fendorf, 2003). As a product of As(III) reduction, As(II) likely substituted for Fe(II) in pyrite structures during the transformation (see below).

The signals of As(V)–O were possibly related to the temporary exposure to air when the samples were transferred to sample chamber during XPS sample preparation. It is reported that oxidation may have occurred at least partially during XPS sample preparation, which involves drying the samples (Bostick and Fendorf, 2003).

3.4. The transfer of As into pyrite

During the transformation, the As(III) previously sorbed by FeS was released into solution along with Fe(II) when FeS dissolved. When pyrite formed, $Fe(II)_{aq}$ was consumed and $As(III)_{aq}$ was incorporated into the newly formed pyrite. The uptake of As by pyrite varied significantly at different temperatures. To examine the impact of temperature on As uptake by pyrite, comparisons between experiments 1 (150 °C) and 3 (80 °C) of pH 7.5 and between experiments 2 (150 °C) and 4 (80 °C) of pH 6.0 were made, respectively. At each $As(III)_0$ concentration, the As content of pyrite in experiment 2 (150 °C) was higher than or equal to that in experiment 4 (80 °C) (Table 1). Similarly, the As content of pyrite in experiment 1 (150 °C) was generally higher than that in experiment 3 (80 °C) (with the exceptions of only experiments 1e versus 3e). This result indicates that the As uptake by pyrite was promoted at high temperature. This promotion may be related to the lattice substitution of As in pyrite, which has been suggested to occur more easily at high temperatures (Riley et al., 2011).

To examine the impact of the pH on As uptake by pyrite, Comparisons between experiments 1 (pH 7.5) and 2 (pH 6.0) of 150 °C and between experiments 3 (pH 7.5) and 4 (pH 6.0) of 80 °C were made, respectively. At each $As(III)_0$ concentration, the As content of pyrite in experiment 2 was higher than that in experiment 1 (Table 1). Similarly, the As content of pyrite in experiment 4 was generally higher than that in experiment 3 (with the exception of only experiments 3e versus 4e). This result indicates that the As uptake by pyrite was enhanced at a low pH.

When FeS transformed to pyrite, the $As(III)_{aq}$ varied differently (Table 1). In experiment 2, the $As(III)_{aq}$ decreased in all five experiment sets, indicating As gain in the solid phases. This can be attributed to the high As uptake by pyrite at high temperature and low pH. In experiments 1, 3, and 4, the $As(III)_{aq}$ increased when the $As(III)_0$ was 3.3–100 mg/L. The As loss from the solid phases is consistent with the lower As uptake ability compared to experiment 2. When the $As(III)_0$ was 1 mg/L, however, the $As(III)_{aq}$ in experiments 1-4a decreased from 100 to below 40 μg/L, indicating that the As uptake ability by pyrite is enough to reduce the $As(III)_{aq}$ in the case of relatively low initial As(III) (~1 mg/L). This finding has implications for the remediation of As contamination. However, our experimental conditions do not reflect natural conditions. To make this result more applicable in water environments, it is required to carry out the transformation experiment and to examine the transfer of As at ambient temperature.

When FeS transformed to pyrite, sorption is a pathway of As incorporation into pyrite (Kirk et al., 2010; Saunders et al., 2018). The XPS analysis showed that As occurred as As(III)–O bonds on the surface of

pyrite, reflecting the sorption of As(III) by pyrite. Wolthers et al. (2005) suggested that As(III) was sorbed by the initially formed pyrite as outer-sphere complexes, whereas Saunders et al. (2018) suggested that both inner-sphere complexation and metal surface site functional groups were probably involved in the sorption of As onto pyrite, providing stable bonds for long-term arsenic retention. When As(III) is sorbed to pyrite, an "arsenopyrite-like" surface precipitate can form (Bostick and Fendorf, 2003). After sorption, As can be incorporated into the pyrite when the pyrite particle grows.

Crystal lattice substitution is another pathway of As uptake by pyrite (Savage et al., 2000; Farquhar et al., 2002). When As is incorporated into pyrite through lattice substitution, the substitution of As(II) for iron and As(–I) for sulfur can occur, resulting in the formation of (Fe, As)S_2 (Chouinard et al., 2005; Qian et al., 2010) and Fe(As,S)$_2$ (Deditius et al., 2008), respectively. More recently, As(II) and As(III) incorporation at octahedral Fe(II) sites and As(–I) incorporation at tetrahedral S(–I) sites during pyrite crystallization at ambient temperature has been reported (Le Pape et al., 2017). The XPS analysis showed that As occurred as As (II)–S bonds on the surface of pyrite of experiments 1 and 2, indicating that the substitution of As(II) for iron might happen at 150 °C. The uptake of As by pyrite through lattice substitution is much higher than that through sorption (Farquhar et al., 2002; Kirk et al., 2010; Saunders et al., 2018). As a result, the content of As in hydrothermal pyrite can be as high as approximately 10.7 wt% (Savage et al., 2000). In experiment 2 (150 °C), the content of As in pyrite reached 12.7%, possibly indicating a significant contribution of lattice substitution of As (Table 1).

The accumulation of As in pyrite varies significantly under different conditions (Saunders et al., 2018). As mentioned above, the incorporation of As into pyrite in this study was promoted at high temperature. Because lattice substitution can lead to a much higher uptake of As in pyrite than sorption (Farquhar et al., 2002; Kirk et al., 2010; Saunders et al., 2018), it is proposed that sorption is the predominant pathway for As uptake by pyrite at relatively low temperature and the lattice substitution of As in pyrite increases with increasing temperature. As a result, the As content of pyrite formed in supergene environments should be lower than that of pyrite formed under hydrothermal conditions. This is consistent with the results of literature that document the concentration of As in pyrites formed under both supergene and hydrothermal conditions (Table 2). As shown in Table 2, most pyrites formed under supergene conditions typically have less than 1.2 wt% As, whereas pyrites formed under hydrothermal conditions usually have a higher As content of more than 2.1 wt%.

4. Conclusions

During the transformation of amorphous FeS to pyrite, dissolution of FeS occurs first prior to pyrite formation. The transformation can be promoted at high temperature and low pH and in the presence of As(III), because both H^+ and As(III) can act as an oxidant that is required in pyrite formation and can promote the generation of $Fe(II)_{aq}$ that is conducive to pyrite formation.

During the transformation, arsenic bound to FeS is first released in the dissolution of FeS and then is incorporated into the newly formed pyrite. Both high temperature and low pH can promote As uptake by pyrite. XPS analysis indicated sorption as a pathway of As incorporation into pyrite. After sorption, As can be incorporated into pyrite when the pyrite particle grows. It is proposed that lattice substitution can be another pathway of As incorporation into pyrite, especially at high temperature. As a result, arsenic lost or gain in solid phases can occur depending on the As uptake ability by pyrite.

Declaration of competing interest

The authors declare that they have no known competing financial interests or personal relationships that could have appeared to influence the work reported in this paper.

Table 2
A summary of As contents in natural pyrites from both supergene and hydrothermal conditions.

		As[a]	Data source
Supergene conditions	Marine sediment	0.93	Huerta-Diaz and Morse (1992)
	Clastic Holocence aquifer	0.62	Saunders et al. (2005)
	River sediment	1.2	Price and Pichler (2006)
	Clastic Holocence aquifer	1.1	Lowers et al. (2007)
	Natural groundwaters	1	Pi et al. (2016)
Hydrothermal conditions	Gold mines	9.6	Wells and Mullens (1973)
	Epithermal Ag–Au deposit	3.1	Griffin et al. (1991)
	Gold deposit	2.2	Arehart et al. (1993)
	Massive sulfide deposits	4.67	Huston et al. (1995)
	Shawmut Mine	2.12	Savage et al. (2000)
	Clio Mine tailings	5	Savage et al. (2000)

[a] Maximum values (wt.%) reported in the references.

Acknowledgements

This study was financially supported by the China National Key Research and Development Program (No. 2017YFD0801000) and the National Natural Science Foundation of China (No. U1612442).

Appendix A. Supplementary data

Supplementary data to this article can be found online at https://doi.org/10.1016/j.apgeochem.2020.104645.

References

Abraitis, P.K., Pattrick, R.A.D., Vaughan, D.J., 2004. Variations in the compositional textural and electrical properties of natural pyrite: a review. Int. J. Miner. Process. 74, 41–59.
Arehart, G.B., Eldridge, C.S., Chryssoulis, S.L., Kesler, S.E., 1993. Ion microprobe determination of sulfur isotope variations in iron sulfides from the Post/Betze sediment hosted disseminated gold deposit, Nevada, USA. Geochem. Cosmochim. Acta 57, 1505–1519.
Bebie, J., Schoonen, M.A.A., Fuhrmann, M., Strongin, D.R., 1998. Surface charge development on transition metal sulfides: an electrokinetic study. Geochem. Cosmochim. Acta 62 (4), 633–642.
Benning, L.G., Wilkin, R.T., Barnes, H.L., 2000. Reaction pathways in the Fe–S system below 100 °C. Chem. Geol. 167, 25–51.
Bostick, B.C., Fendorf, S., 2003. Arsenite sorption on troilite (FeS) and pyrite (FeS_2). Geochem. Cosmochim. Acta 67 (5), 909–921.
Butler, I.B., Rickard, D., 2000. Framboidal pyrite formation via the oxidation of iron(II) monosulfide by hydrogen sulphide. Geochem. Cosmochim. Acta 64, 2665–2672.
Chouinard, A., Paquette, J., Williams-Jones, A.E., 2005. Crystallographic controls on trace-element incorporation in auriferous pyrite from the Pascua epithermal high-sulfidation deposit, Chile-Argentina. Can. Mineral. 43, 951–963.
Deditius, A.P., Utsunomiya, S., Renock, D., Ewing, T.C., Ramana, C.V., Becker, U., Kesler, S.E., 2008. A proposed new type of arsenian pyrite: composition, nanostructure and geological significance. Geochem. Cosmochim. Acta 72 (12), 2919–2933.
Farquhar, M.L., Charnock, J.M., Livens, F.R., Vaughan, D.J., 2002. Mechanisms of arsenic uptake from aqueous solution by interaction with goethite, lepidocrocite, mackinawite, and pyrite: an X-ray absorption spectroscopy study. Environ. Sci. Technol. 36 (8), 1757–1762.
Fu, Z., Zhang, G., Li, H., Chen, J., Liu, F., Wu, Q., 2016. Influence of reducing conditions on the release of antimony and arsenic from a tailing sediment. J. Soils Sediments 16, 2471–2481.
Gallegos, T.J., Hyun, S.P., Hayes, K.F., 2007. Spectroscopic investigation of the uptake of arsenite from solution by synthetic mackinawite. Environ. Sci. Technol. 41, 7781–7786.
Gallegos, T.J., Han, Y.S., Hayes, K.F., 2008. Model predictions of realgar precipitation by reaction of As(III) with synthetic mackinawite under anoxic conditions. Environ. Sci. Technol. 42, 9338–9343.
Goldhaber, M.B., Kaplan, I.R., 1974. The sulfur cycle. In: Goldberg, E.D. (Ed.), The Sea, 5. Wiley, pp. 569–655. Chap. 17.

Griffin, W.L., Ashley, P.M., Ryan, C.G., Soey, H.S., Suter, G.F., 1991. Pyrite geochemistry in the North Arm epithermal Ag –Au deposit, Queensland, Australia: a proton-microprobe study. Can. Mineral. 29, 185–198.
Han, Y.-S., Gallegos, T.J., Demond, A.H., Hayes, K.F., 2011. FeS-coated sand for removal of arsenic(III) under anaerobic conditions in permeable reactive barriers. Water Res. 45, 593–604.
Han, D.S., Batchelor, B., Abdel-Wahab, A., 2013. XPS analysis of sorption of selenium(IV) and selenium(VI) to mackinawite (FeS). Environ. Prog. Sustain. 32 (1), 84–93.
Han, Y.-S., Lee, C.M., Chon, C.M., Kwon, J.A., Park, J.H., Shin, Y.J., Lim, D.H., 2018. Enhanced oxidation resistance of $NaBH_4$-treated mackinawite (FeS): application to Cr(Vl) and As(III) removal. Chem. Eng. J. 353, 890–899.
Huerta-Diaz, M.A., Morse, J.W., 1992. The pyritization of trace metals in anoxic marine sediments. Geochem. Cosmochim. Acta 56, 2681–2702.
Huston, D.L., Sie, S.H., Suter, G.F., Cooke, D.R., Both, R.A., 1995. Trace elements in sulfide minerals from Eastern Australian volcanic-hosted massive sulfide deposits: Part 1. Proton microprobe analyses of pyrite, chalcopyrite and sphalerite, and Part II. Selenium levels in pyrite: comparison with ($\delta^{34}S$ values and implications for the source of sulfur in volcanogenic hydrothermal systems. Econ. Geol. 90, 1167–1196.
Jeong, H.Y., Lee, J.H., Hayes, K.F., 2008. Characterization of synthetic nanocrystalline mackinawite: crystal structure, particle size, and specific surface area. Geochem. Cosmochim. Acta 72, 493–505.
Kim, E.J., Batchelor, B., 2009. Macroscopic and X-ray photoelectron spectroscopic investigation of interactions of arsenic with synthesized pyrite. Environ. Sci. Technol. 43, 2899–2904.
Kirk, M.F., Roden, E.E., Crossey, L.J., Brearley, A.J., Spilde, M.N., 2010. Experimental analysis of arsenic precipitation during microbial sulfate and iron reduction in model aquifer sediment reactors. Geochem. Cosmochim. Acta 74, 2538–2555.
Lamer, V.K., 1952. Nucleation in phase transitions. Ind. Eng. Chem. 44 (6), 1270–1277.
Lan, Y., Butler, E.C., 2014. Monitoring the transformation of mackinawite to greigite and pyrite on polymer supports. Appl. Geochem. 50, 1–6.
Le Pape, P., Blanchard, M., Brest, J., Boulliard, J.C., Ikogou, M., Stetten, L., Wang, S., Landrot, G., Morin, G., 2017. Arsenic incorporation in pyrite at ambient temperature at both tetrahedral S-I and octahedral Fe-II site: evidence from EXAFS-DFT analysis. Environ. Sci. Technol. 51 (1), 150–158.
Licht, S., Hodes, G., Manassen, J., 1986. Numerical analysis of aqueous polysulfide solutions and its application to cadmium chalcogenide/polysulfide photoelectrochemical solar cells. Inorg. Chem. 25, 2486–2489.
Lowers, H.A., Breit, G.N., Foster, A.L., Whitney, J., Yount, J., Uddin, M.N., Muneem, A. A., 2007. Arsenic incorporation into authigenic pyrite, Bengal Basin sediment. Bangladesh. Geochim. Cosmochim. Acta 71, 2699–2717.
Maguffin, S.C., Jin, Q., 2018. Testing biostimulated sulfate reduction as a strategy of arsenic remediation in iron-rich aquifers. Chem. Geol. 493, 80–86.
Morse, J.W., Arakaki, T., 1993. Adsorption and coprecipitation of divalent metals with mackinawite (FeS). Geochem. Cosmochim. Acta 57, 3635–3640.
Nesbitt, H.W., Muir, I.J., 1998. Oxidation states and speciation of secondary products on pyrite and arsenopyrite reacted with mine waste waters and air. Mineral. Petrol. 62, 123–144.
Ohfuji, H., Rickard, D., 2005. Experimental syntheses of framboids - a review. Earth Sci. Rev. 71, 147–170.
Peiffer, S., Behrends, T., Hellige, K., Larese-Casanova, P., Wan, M., Pollok, K., 2015. Pyrite formation and mineral transformation pathways upon sulfidation of ferric hydroxides depend on mineral type and sulfide concentration. Chem. Geol. 400, 44–55.
Pi, K., Wang, Y., Xie, X., Ma, T., Su, C., Liu, Y., 2016. Role of sulfur redox cycling on arsenic mobilization in aquifers of Datong Basin, northern China. Appl. Geochem. 71, 31–43.
Price, R.E., Pichler, T., 2006. Abundance and mineralogical association of arsenic in the Suwannee Limestone (Florida): implications for arsenic release during water–rock interaction. Chem. Geol. 228, 44–56.
Qian, G.J., Brugger, J., Skinner, W.M., Chen, G.R., Pring, A., 2010. An experimental study of the mechanism of the replacement of magnetite by pyrite up to 300°C. Geochem. Cosmochim. Acta 74, 5610–5630.
Renock, D., Gallegos, T., Utsunomiya, S., Hayes, K., Ewing, R.C., Becker, U., 2009. Chemical and structural characterization of as immobilization by nanoparticles of mackinawite (FeS_m). Chem. Geol. 268, 116–125.
Rickard, D., 1975. Kinetics and mechanism of pyrite formation at low temperatures. Am. J. Sci. 275, 636–652.
Rickard, D., 1995. Kinetics of FeS precipitation: Part 1. Competing reaction mechanisms. Geochem. Cosmochim. Acta 59, 4367–4379.
Rickard, D., 1997. Kinetics of pyrite formation by the H_2S oxidation of iron (II) monosulfide in aqueous solutions between 25°C and 125°C: the rate equation. Geochem. Cosmochim. Acta 61, 115–134.
Rickard, D., Morse, J.W., 2005. Acid volatile sulfide (AVS). Mar. Chem. 97 (3–4), 141–197.
Rickard, D., 2006. The solubility of FeS. Geochem. Cosmochim. Acta 70 (23), 5779–5789.
Rickard, D., Grimes, S., Butler, I., Oldroyd, A., Davies, K.L., 2007. Botanical constraints on pyrite formation. Chem. Geol. 236, 228–246.
Rickard, D., 2019. How long does it take a pyrite framboid to form? Earth Planet Sci. Lett. 513, 64–68.
Riley, K.W., French, D.H., Farrell, O.P., Wood, R.A., Huggins, F.E., 2011. Modes of occurrence of trace and minor elements in some Australian coals. Int. J. Coal Geol. 94, 214–224.
Saunders, J.A., Mohammad, S., Korte, N.E., Lee, M.K., Fayek, M., Castle, D., Barnett, M. O., 2005. Groundwater geochemistry, microbiology, and mineralogy of two arsenic-bearing Holocene alluvial aquifers from the USA. In: ODay, P.A., Vlassopoulos, D., Ming, X., Benning, L.G. (Eds.), Advances in Arsenic Research: Integration of Experimental and Observational Studies and Implications for Mitigation. Am. Chem. Soc. Symposium Series, 915, pp. 191–205.
Saunders, J.A., Lee, M.K., Dhakal, P., Ghandehari, S.S., Wilson, T., Billor, M.Z., Uddin, A., 2018. Bioremediation of arsenic-contaminated groundwater by sequestration of arsenic in biogenic pyrite. Appl. Geochem. 96, 233–243.
Savage, K.S., Tingle, T.N., O'Day, P.A., Waychunas, G.A., Bird, D.K., 2000. Arsenic speciation in pyrite and secondary weathering phases, mother lode gold district, tuolumne county, California. Appl. Geochem. 15 (8), 1219–1244.
Schoonen, M.A.A., Barnes, H.L., 1991. Reactions forming pyrite: I. Nucleation of FeS_2 below 100°C. Geochem. Cosmochim. Acta 55, 1495–1504.
Stanton, M.R., Goldhaber, M.B., 1991. An experimental study of goethite sulfidization: relationships to the diagenesis of iron and sulfur. In: Tuttle, M.L., Chep, E. (Eds.), Geochemical, Biochemical, and Sedimentological Studies of the Green River Formation, Wyoming, Utah, and Colorado. USGS Bull., 1973.
Swanner, E.D., Webb, S.M., Kappler, A., 2019. Fate of cobalt and nickel in mackinawite during diagenetic pyrite formation. Am. Mineral. 104, 917–928.
Watson, J.H.P., Ellwood, D.C., Deng, Q., Mikhalowsky, S., Hayter, C.E., Evans, J., 1995. Heavy metal adsorption on bacterially produced FeS. Miner. Eng. 8, 1097–1108.
Webster, J.G., 1990. The solubility of As_2S_3 and speciation of as in dilute and sulfide-bearing fluids at 25°C and 90°C. Geochem. Cosmochim. Acta 54, 1009–1017.
Wells, J.D., Mullens, T.E., 1973. Gold-bearing arsenian pyrite determined by microprobe analysis, Cortez and Carlin gold mines, Nevada. Econ. Geol. 68, 187–201.
Wilkin, R.T., Barnes, H.L., 1996. Pyrite formation by reactions of iron monosulfides with dissolved inorganic and organic sulfur species. Geochem. Cosmochim. Acta 60, 4167–4179.
Wilkin, R.T., Barnes, H.L., 1997. Formation processes of framboidal pyrite. Geochem. Cosmochim. Acta 61 (2), 323–339.
Wilkin, R.T., Ford, R.G., 2002. Use of hydrochloric acid for determining solid-phase arsenic partitioning in sulfidic sediments. Environ. Sci. Technol. 36, 4921–4927.
Wolthers, M., van der Gaast, S.J., Rickard, D., 2003. The structure of disordered mackinawite. Am. Mineral. 88, 2007–2015.
Wolthers, M., Charlet, L., van Der Linde, P.R., Rickard, D., van Der Weijden, C.H., 2005. Surface chemistry of disordered mackinawite (FeS). Geochem. Cosmochim. Acta 69 (14), 3469–3481.
Wolthers, M., Butler, I.B., Rickard, D., 2007. Influence of arsenic on iron sulfide transformations. Chem. Geol. 236, 217–227.
Xie, X., Liu, Y., Pi, K., Liu, C., Li, J., Duan, M., Wang, Y., 2016. In situ Fe-sulfide coating for arsenic removal under reducing conditions. J. Hydrol 534, 42–49.